Modeling of Wave Propagation in Inhomogeneous Media

Dirk-Jan van Manen* and Johan O. A. Robertsson
WesternGeco Oslo Technology Centre, Solbraveien 23, 1383 Asker, Norway

Andrew Curtis
School of GeoSciences, University of Edinburgh, Grant Institute, West Mains Road, Edinburgh EH9 3JW, United Kingdom
(Received 8 February 2005; published 27 April 2005)

We present a methodology providing a new perspective on modeling and inversion of wave propagation satisfying time-reversal invariance and reciprocity in generally inhomogeneous media. The approach relies on a representation theorem of the wave equation to express the Green function between points in the interior as an integral over the response in those points due to sources on a surface surrounding the medium. Following a predictable initial computational effort, Green's functions between arbitrary points in the medium can be computed as needed using a simple cross-correlation algorithm.

DOI: 10.1103/PhysRevLett.94.164301 PACS numbers: 43.20.+g, 43.60.+d

Introduction.—Many applications in diverse fields such as communications analysis, waveform inversion, imaging, survey and experimental design, and industrial design require a large number of modeled solutions of the wave equation in different media. The most complete methods of solution, such as finite differences (FD), which accurately model all high-order interactions between scatterers in a medium, typically become prohibitively expensive for realistically complete descriptions of complex media and the geometries of sources and receivers and hence for solving realistic problems based on the wave equation. Here we show that the key to breaking this apparent paradigm lies in a basic reciprocity argument in combination with recent theoretical advances in the fields of time-reversed acoustics [1] and seismic interferometry [2–5].

In time-reversed acoustics, invariance of the wave equation for time reversal can be exploited to focus a wave field through a highly scattering medium on an original source point [6]. Cassereau and Fink [7,8] realized that the acoustic representation theorem [9] can be used to time reverse a wave field in a volume by creating secondary sources (monopole and dipole) on a surface surrounding the medium such that the boundary conditions correspond to the time-reversed components of a wave field measured there. These secondary sources give rise to the backpropagating, time-reversed wave field inside the medium that collapses onto itself at the original source location. Note that since there is no source term absorbing the converging wave field, the size of the focal spot is limited to half a (dominant) wavelength in accordance with diffraction theory [7]. The diffraction limit was overcome experimentally by de Rosny and Fink [10] by introducing the concept of an ''acoustic sink.''

In interferometry, waves recorded at two receiver locations are correlated to find the Green function between the locations. Interferometry has been successfully applied to helioseismology [11], ultrasonics [2], and exploration seismics [3]. Recently it was shown that there exists a close link between the time-reversed acoustics and interferometry disciplines when Derode *et al.* [1] analyzed the emergence of the Green function from field-field correlations in an open scattering medium in terms of time-reversal symmetry. The Green function can be recovered as long as the sources in the medium are distributed forming a perfect time-reversal device. A rigorous proof for the general case of an arbitrary inhomogeneous elastic medium was presented by Wapenaar [4].

Theory and method.—Our starting point is the acoustic wave equation in the space-frequency domain: $\partial_i(\rho^{-1}\partial_i p) + (\omega^2/\kappa)p = f$, where $p = p(\boldsymbol{x}, \omega)$ denotes the pressure field at location $\boldsymbol{x}$ and frequency ω, $\rho(\boldsymbol{x})$, and $\kappa(\boldsymbol{x})$ denote the mass density and incompressibility, respectively, and $f = f(\boldsymbol{x}, \omega)$ is a source term, denoting the change of volume injection rate density over time. Now consider two states A and B that could occur in the same medium independently: $\partial_i(\rho^{-1}\partial_i p^A) + (\omega^2/\kappa)p^A = f^A$ and $\partial_i(\rho^{-1}\partial_i p^B) + (\omega^2/\kappa)p^B = f^B$. The acoustic representation theorem can be derived by multiplying the equation for the first state by $p^B(\boldsymbol{x}, \omega)$ and the equation for the second state by $p^A(\boldsymbol{x}, \omega)$, subtracting and integrating the results over a volume V, applying Gauss's theorem to convert the volume integral to a surface integral and identifying state A with a mathematical state [i.e., a state involving (analytic) Green's functions rather than measured quantities [9]]: $f^A(\boldsymbol{x}) = \delta(\boldsymbol{x} - \boldsymbol{x}')$ and $p^A(\boldsymbol{x}) = G(\boldsymbol{x}, \boldsymbol{x}')$, where $\delta(\boldsymbol{x})$ denotes the Dirac delta distribution and $G(\boldsymbol{x}, \boldsymbol{x}')$ Green's function due to a source at $\boldsymbol{x}'$. Following a reciprocity argument, interchanging the coordinates $\boldsymbol{x} \leftrightarrow \boldsymbol{x}'$ and dropping the superscripts for state B, this procedure yields

$$p(\boldsymbol{x}) = \int_V G(\boldsymbol{x}, \boldsymbol{x}')f(\boldsymbol{x}')dV' + \int_S \frac{1}{\rho(\boldsymbol{x}')}[\nabla' G(\boldsymbol{x}, \boldsymbol{x}')p(\boldsymbol{x}') - G(\boldsymbol{x}, \boldsymbol{x}')\nabla' p(\boldsymbol{x}')] \cdot \boldsymbol{n}\, dS', \quad (1)$$

where $\nabla' G(\boldsymbol{x}, \boldsymbol{x}')$ denotes the gradient of the Green func-

tion with respect to primed coordinates and $\boldsymbol{n}$ denotes the normal to the boundary. Thus, the wave field can be computed everywhere inside the volume V once the source $f(\boldsymbol{x}')$ inside the volume and both the wave field $p(\boldsymbol{x}')$ and its gradient $\boldsymbol{\nabla}' p(\boldsymbol{x}')$ on the surrounding surface S are known. To time reverse a wave field in a volume V, the wave field p and its gradient $\boldsymbol{\nabla}' p$, measured at the surface S in a first step have to be time reversed on the surface such that the time-reversed pressure field $p_{\mathrm{tr}}(\boldsymbol{x})$ radiated from the boundary can be written

$$p_{\mathrm{tr}}(\boldsymbol{x}) = \int_S \frac{1}{\rho(\boldsymbol{x}')}[\boldsymbol{\nabla}' G(\boldsymbol{x}, \boldsymbol{x}') p^*(\boldsymbol{x}') - G(\boldsymbol{x}, \boldsymbol{x}')\boldsymbol{\nabla}' p^*(\boldsymbol{x}')] \cdot \boldsymbol{n} dS', \quad (2)$$

where an asterisk denotes complex conjugation, and we have ignored the volume integral which corresponds to the acoustic sink [10]. Note that Eq. (2) can be used to compute the time-reversed wave field (including all high-order interactions) at any location, not just at an original source location. Now, assume that the wave field $p(\boldsymbol{x}')$ was due to a point source at location $\boldsymbol{x}_1$ and that we have $p(\boldsymbol{x}') = G(\boldsymbol{x}', \boldsymbol{x}_1)$. By measuring the wave field in a second location $\boldsymbol{x}_2$, the Green function and its time reverse between the source point $\boldsymbol{x}_1$ and the second point $\boldsymbol{x}_2$ are observed [1,4]:

$$G^*(\boldsymbol{x}_2, \boldsymbol{x}_1) - G(\boldsymbol{x}_2, \boldsymbol{x}_1) = \int_S \frac{1}{\rho(\boldsymbol{x}')}[\boldsymbol{\nabla}' G(\boldsymbol{x}_2, \boldsymbol{x}') G^*(\boldsymbol{x}', \boldsymbol{x}_1) - G(\boldsymbol{x}_2, \boldsymbol{x}')\boldsymbol{\nabla}' G^*(\boldsymbol{x}', \boldsymbol{x}_1)] \cdot \boldsymbol{n} dS', \quad (3)$$

where the negative forward Green function $-G(\boldsymbol{x}_2, \boldsymbol{x}_1)$ arises from the missing acoustic sink [7,10]. Using reciprocity, we can rewrite Eq. (3) so that it involves only sources on the boundary enclosing the medium:

$$G^*(\boldsymbol{x}_2, \boldsymbol{x}_1) - G(\boldsymbol{x}_2, \boldsymbol{x}_1) = \int_S \frac{1}{\rho(\boldsymbol{x}')}[\boldsymbol{\nabla}' G(\boldsymbol{x}_2, \boldsymbol{x}') G^*(\boldsymbol{x}_1, \boldsymbol{x}') - G(\boldsymbol{x}_2, \boldsymbol{x}')\boldsymbol{\nabla}' G^*(\boldsymbol{x}_1, \boldsymbol{x}')] \cdot \boldsymbol{n} dS'. \quad (4)$$

Thus, the Green function between two points $\boldsymbol{x}_1$ and $\boldsymbol{x}_2$ can be calculated once the Green functions between the enclosing boundary and these points are known.

A highly efficient two-stage modeling strategy follows from Eq. (4): first, the Green function terms G and $\boldsymbol{\nabla}' G$ are calculated from boundary locations to internal points in a conventional forward modeling phase; in a second intercorrelation phase, the integral is calculated requiring only cross correlations and numerical integration. Since the computational cost of typical forward modeling algorithms (e.g., FD) does not significantly depend on the number of receiver locations but mainly on the number of source locations, efficiency and flexibility are achieved by storing the wave field modeled for each of the boundary sources in as many points as possible throughout the medium. To calculate the Green function between two points the recordings in the first point due to the dipole sources on the boundary are cross correlated with the recordings in the second point due to the monopole sources, and vice versa. The resulting cross correlations are subtracted and numerically integrated over the boundary of source locations. Unprecedented flexibility follows from the fact that the Green function can be calculated between all pairs of points that were defined up front and stored in the initial modeling phase. Thus, we calculate a partial modeling solution that is common to all Green functions, then a bespoke component for each Green function.

Results.—Our method is illustrated using a FD implementation of the two-dimensional acoustic wave equation for a typical modeling scenario in an exploration seismic setting. In Fig. 1 the compressional wave velocity in a 4.6×4.6 km representative region of an Earth model often used to benchmark marine seismic imaging algorithms [12] is shown. Note the high velocity (4500 m/s) salt body on the right. In black, two points of interest (offset 1 km) are shown. The dotted line denotes the boundary with $N_S = 912$ source locations distributed with a density consistent with the local spatial Nyquist frequency. Outgoing (i.e., radiation or absorbing) boundary conditions [13] are applied right outside the surface enclosing the points of interest to truncate the computational domain.

Forward simulations were carried out for each of the 912 source locations on the boundary and the waveforms stored at 90 000 points distributed throughout the model. Note that because of the cross symmetry of the terms in the integrand in Eq. (4), no sources are required along interfaces with homogeneous boundary conditions (e.g., the Earth's free surface). Depending on the particular wave equation (scalar or vector), several forward simulations may have to be carried out for each source location. In the acoustic example two data sets are required: with

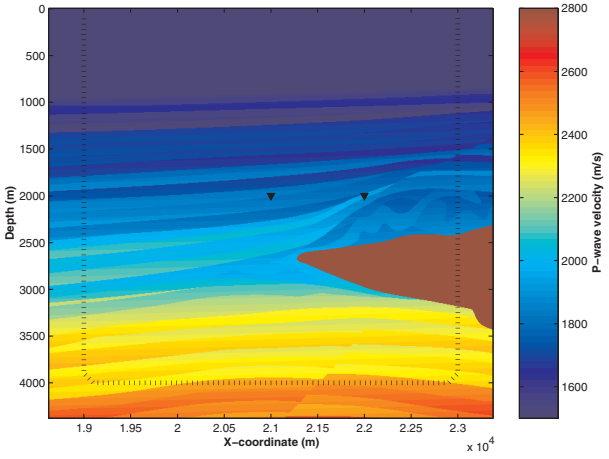

FIG. 1 (color). 2D acoustic marine seismic model (compressional velocity) [12]. The color scale is clipped to display weak velocity contrasts (velocity of salt is 4500 m/s).

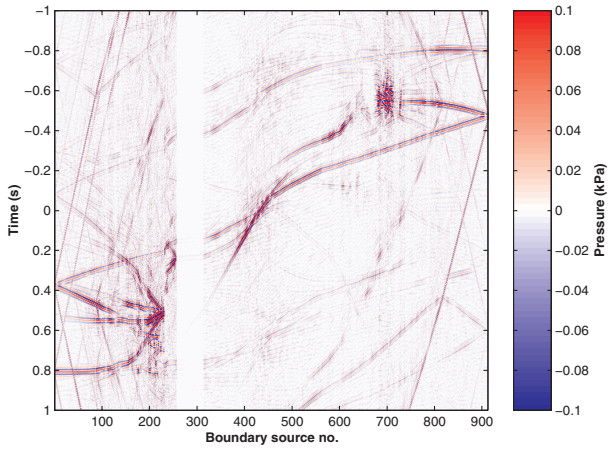

FIG. 2 (color). Green's function intercorrelation gather (weighted) for the two points shown in Fig. 1. The low correlation amplitude for boundary sources 250–310 corresponds to the shadow of the salt body.

monopole and dipole sources, respectively. However, when the surface surrounding the medium has outgoing boundary conditions, the wave field and its gradient (traction) are directly related [14]. Hence, the normal derivatives can be calculated from the wave field itself without additional modeling. Figure 2 shows the integrand of Eq. (4), inversely weighted by boundary source density, for each source location $\boldsymbol{x}'$ and for the two points $\boldsymbol{x}_1$ and $\boldsymbol{x}_2$ in Fig. 1. In Fig. 3, the resulting Green function between the points in Fig. 1 computed using Eq. (4), and a reference trace computed by direct FD modeling, are shown in red and blue, respectively. The signal at negative times corresponds to the waves flowing back in time and the opposite direction past the second point. The four insets show the excellent match between the reference trace and the new method in detail.

Interestingly, the time series in Fig. 2 bear little resemblance to the final Green function in Fig. 3. Equation (4) sums these signals along the horizontal axis and hence relies on the delicate constructive and destructive interference of time-reversed waves backpropagating through the medium, recombining and undoing the scattering at every discontinuity to produce the Green function.

In Fig. 2, each column represents the set of all waves traveling from point $\boldsymbol{x}_1$ to a single boundary source, correlated with the Green function from that boundary source to $\boldsymbol{x}_2$. Some of the waves traveling from $\boldsymbol{x}_1$ to this boundary source may pass through $\boldsymbol{x}_2$ before being recorded and therefore have the remainder of their path in common with waves emitted from $\boldsymbol{x}_2$ in the same direction (or wave number). The travel times associated with such identical parts of the path are eliminated in the cross correlation and the remaining part corresponds to an event in the Green function from $\boldsymbol{x}_1$ to $\boldsymbol{x}_2$. Similarly, some waves emitted from $\boldsymbol{x}_2$ may travel to the boundary source location via $\boldsymbol{x}_1$ and have a common section of path between $\boldsymbol{x}_1$ and the boundary source. Again travel time on the common section will be eliminated and give rise to the same event in the Green function from $\boldsymbol{x}_1$ to $\boldsymbol{x}_2$ at negative (acausal) times. Note that the vector wave numbers involved for positive and negative times are in general not parallel since they are related to the background structure of the whole model (one or the other may not exist for the same boundary source). Hence, waves at positive and negative times are

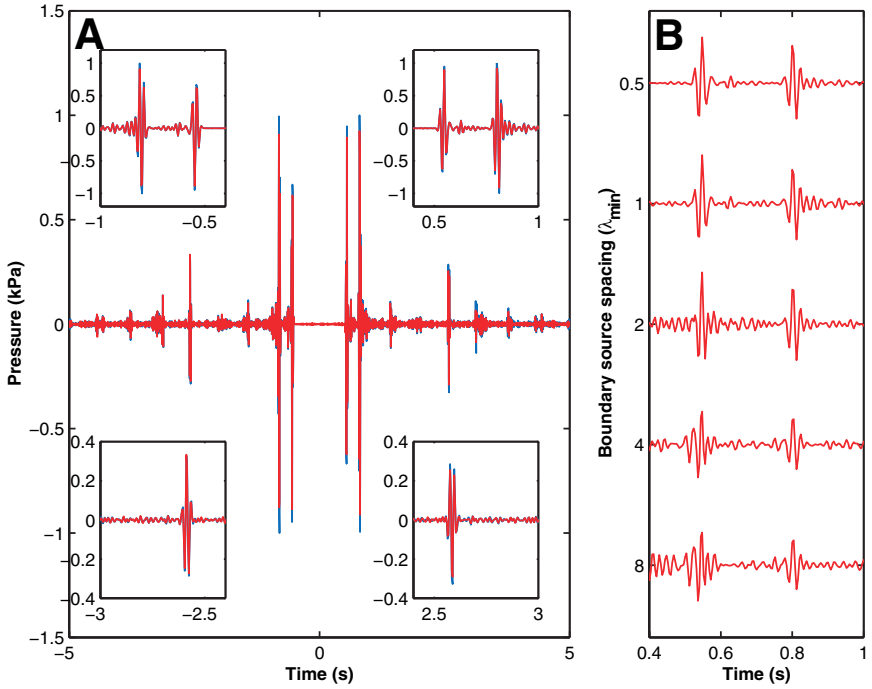

FIG. 3 (color). (a) Waveform computed by summation of the weighted intercorrelation gather shown in Fig. 2 (red) compared to a conventional FD computation (blue). The insets show particular events in the time series. (b) Waveform computed after successive subsampling of the intercorrelation gather.

reconstructed differently. All cross correlations involving energy that does not pass through $\boldsymbol{x}_2$ are eliminated by destructive interference by the summation of the columns [15].

The new method is particularly attractive in applications where Green's functions are desired between a large number of points interior to a medium, but where there are few common sources or receiver points. No other existing method could offer full waveforms at comparable computational cost. The method also offers great flexibility where the exact interior points are not known in advance since Green's functions can be computed on an ''as needed'' basis from Green's functions between points on the surrounding surface and its interior. We have shown how the latter Green functions constitute a common component of all Green's functions in the medium through Eq. (4). In the example above, this common component is stored compressed by a factor of 50 compared to explicitly storing all desired Green's functions between pairs of interior points.

Whereas traditional approximate modeling methods typically impose restrictions with respect to the degree of heterogeneity in the medium of propagation or neglect high-order scattering, the new time-reversal modeling methodology allows us instead to compromise on the noise level while maintaining high-order scattering and full heterogeneity in the medium. Recent experimental and theoretical work indicates that time-reversed imaging is robust with respect to perturbations in the boundary conditions [1,16]. For cases where the wave propagation is heavily dominated by multiple scattering even a single source may be sufficient to refocus the essential parts of a time-reversed signal [17]. Also for more deterministic models, such as the one in the example, it is possible to substantially reduce the number of sources and still recover the essential parts of the signal. In Fig. 3(b) we show the part of the signal corresponding to the inset in the upper right corner of Fig. 3(a) as we reduce the number of sources around the boundary. Even for as few as $\frac{1}{16}$ of the original number of sources we are able to reproduce amplitude and phase of an arrival of interest fairly accurately, but with an increased noise level. Clearly, the required number of sources will depend on the application. Our numerical experiments thus confirm the robustness of the methodology with respect to variations in parameters such as location and discretization of integration surfaces.

We also experimented with exciting the boundary sources simultaneously by encoding the source signals using pseudonoise sequences [18] and with simultaneous sources distributed randomly in the medium [1] as two alternative ways to reduce the number of sources. There is a well-known limit to the quality of separation of such sequences of a given length when emitted simultaneously [19]. Insufficient separation of sequences again is manifest in an increased noise level in the final Green functions. In all cases, the limits of separation caused relatively high noise levels compared to the equivalent FD effort using the method described above.

Thus, we have shown how recent insight into the relationship between Green's theorem and time reversal can be extended to the modeling of wave propagation by invoking reciprocity. We expect that this may significantly change the way we approach modeling and inversion of the wave equation in future.

We would like to thank Roel Snieder for alerting us to possible redundancy in the boundary sources, which was tested using successive downsampling.

*Electronic address: DManen@oslo.westerngeco.slb.com

[1] A. Derode, E. Larose, M. Tanter, J. de Rosny, A. Tourin, M. Campillo, and M. Fink, J. Acoust. Soc. Am. **113**, 2973 (2003).
[2] R. L. Weaver and O. I. Lobkis, Phys. Rev. Lett. **87**, 134301 (2001).
[3] K. Wapenaar, D. Draganov, J. Thorbecke, and J. Fokkema, Geophys. J. Int. **156**, 179 (2004).
[4] K. Wapenaar, Phys. Rev. Lett. **93**, 254301 (2004).
[5] G. T. Schuster, in *Extended Abstracts of the 63rd Annual International Meeting of the European Association of Geoscientists and Engineers* (European Association of Geoscientists and Engineers, Houten, The Netherlands, 2001), p. A-32.
[6] A. Derode, P. Roux, and M. Fink, Phys. Rev. Lett. **75**, 4206 (1995).
[7] D. Cassereau and M. Fink, IEEE Trans. Ultrason. Ferroelectr. Freq. Control **39**, 579 (1992).
[8] D. Cassereau and M. Fink, J. Acoust. Soc. Am. **94**, 2373 (1993).
[9] K. Wapenaar and J. Fokkema, J. Appl. Mech. **71**, 145 (2004).
[10] J. de Rosny and M. Fink, Phys. Rev. Lett. **89**, 124301 (2002).
[11] J. E. Rickett and J. F. Claerbout, Sol. Phys. **192**, 203 (2000).
[12] D. Stoughton, J. Stefani, and S. Michell, in *Expanded Abstracts of the 71st Annual International Meeting of the Society of Exploration Geophysicists* (Society of Exploration Geophysicists, Tulsa, OK, 2001), p. 1269.
[13] R. Clayton and B. Engquist, Bull. Seismol. Soc. Am. **67**, 1529 (1977).
[14] E. Holvik, Ph.D. thesis, NTNU Trondheim, Norway, 2003.
[15] R. Snieder, Phys. Rev. E **69**, 46610 (2004).
[16] R. Snieder and J. A. Scales, Phys. Rev. E **58**, 5668 (1998).
[17] C. Draeger and M. Fink, J. Acoust. Soc. Am. **105**, 611 (1999).
[18] P. Fan and M. Darnell, *Sequence Design for Communications Applications* (Research Studies Press, Hertfordshire, UK, 2003).
[19] L. R. Welch, IEEE Trans. Inf. Theory **20**, 397 (1974).